SANDIA REPORT
SAND2019-12669
Printed October 2019

Sandia National Laboratories

Finite-element modeling for an explosively loaded ferroelectric generator

John H. J. Niederhaus, Pin Yang, and Christopher DiAntonio
Sandia National Laboratories
Albuquerque, NM 87185

George B. Vunni
CCDC Army Research Laboratory
Aberdeen Proving Ground, MD 21005

Prepared by
Sandia National Laboratories
Albuquerque, New Mexico
87185 and Livermore,
California 94550

Issued by Sandia National Laboratories, operated for the United States Department of Energy by National Technology & Engineering Solutions of Sandia, LLC.

Available to DOE and DOE contractors from
U.S. Department of Energy
Office of Scientific and Technical Information
P.O. Box 62
Oak Ridge, TN 37831

Telephone: (865) 576-8401
Facsimile: (865) 576-5728
E-Mail: reports@osti.gov
Online ordering: http://www.osti.gov/scitech

Available to the public from
U.S. Department of Commerce
National Technical Information Service
5301 Shawnee Rd
Alexandria, VA 22312

Telephone: (800) 553-6847
Facsimile: (703) 605-6900
E-Mail: orders@ntis.gov
Online order: https://classic.ntis.gov/help/order-methods/

ABSTRACT

A preliminary finite-element model has been developed using the ALEGRA-FE code for explosive-driven depoling of a PZT 95/5 ferroelectric generator. The ferroelectric material is characterized using hysteresis-loop and hydrostatic depoling tests. These characteristics are incorporated into ALEGRA-FE simulations that model the explosive drive mechanism and shock environment in the material leading to depoling, as well as the ferroelectric response and the behavior of a coupled circuit. The ferroelectric-to-antiferroelectric phase transition is captured, producing an output voltage pulse that matches experimental data to within 10% in rise time, and to within about 15% for the final voltage. Both experimental and modeled pulse magnitudes are less than the theoretical maximum output of the material. Observations from materials characterization suggest that unmodeled effects such as trapped charge in the stored FEG material may have influenced the experimentally observed output.

ACKNOWLEDGEMENTS

The authors are thankful to Mr. Peter Bartkowski and Mr. Paul Berning at ARL for initiating this work and providing critical insight along the way.

Also, we thank Dr. Thomas Hughes and Dr. James Carleton at Sandia for important technical discussions and guidance.

Finally, we wish to thank Tom Chavez at Sandia, who was heavily involved in conducting the laboratory materials characterization.

CONTENTS

1. Introduction and background 9
2. Review of previous experimental tests 10
3. PZT 95/5 characterization testing 13
   3.1. P-E hysteresis looping 13
   3.2. Hydrostatic depoling 15
   3.3. P-E hysteresis looping after hydrostatic depoling 16
4. ALEGRA-FE modeling 18
   4.1. The ALEGRA-FE code 18
   4.2. The FE AFE Ceramic model 19
   4.3. Simulation mesh and input parameters 23
   4.4. Simulation material properties 24
   4.5. Caveats related to the simulations 26
5. Simulation results 27
6. Conclusions 33

LIST OF FIGURES

Figure 1: Reproduced from Bartkowski and Berning (2017) [1]: layout of "edge"-configuration tests (not to scale) with inset photograph of FEG bar and overlaid dashed arrows indicating the direction of the average remanent polarization direction. 10
Figure 2: Reproduced from Bartkowski and Berning (2017) [1]: capacitor charging by FEG depoling, from the three successful shots in lateral orientation from the BB2017 experiments. 12
Figure 3: FEG sample after cutting into four pieces. The topmost sample shows evidence of possible electrocoloration [9]. 13
Figure 4: P-E hysteresis loop for one PZT 95/5 sample. 14
Figure 5: Hydrostatic depoling curve for one PZT 95/5 sample. 15
Figure 6: P-E hysteresis loop test after hydrostatic depoling. 16
Figure 7: Notional orientation of the polarization vector in ferroelectric domains within a single grain of ferroelectric material in the unpoled (left) and poled (right) states. 20
Figure 8: FE-AFE Ceramic model discretization methods for stochastic orientations of the dipoles or polarization vector: (left) NBINS approach and (right) REFINE approach. Taken from Reference [20]. 20
Figure 9: Notional representation of the dipoles or polarization vector in ferroelectric domains within a single grain of ferroelectric material in the FE (left) and AFE (right) states. 22
Figure 10: ALEGRA-FE simulation geometry and mesh. The mesh has been coarsened for visibility. 23
Figure 11: Circuit network used in ALEGRA-FE simulations. 24

Figure 12: Material motion in ALEGRA-FE simulations using configuration 1. Yellow: explosive (discarded at $t = 25$ μs). Green: fiberglass modeled as PMMA. Gray: steel. Purple: aluminum. Pink: PZT. 27
Figure 13: Mechanical polarization y-component evolution during shock traversal over the FEG. 28
Figure 14: Measured and simulated capacitor voltage history during FEG depoling, with simulated voltages measured (left) on the FEG output terminal and (right) across the capacitor. Measured data are from the three "edge" shots from BB2017 [1]. 29
Figure 15: Capacitor voltage from simulations with reduced values of remanent polarization. 31
Figure 16: Time history data from a diagnostic tracer point in the FEG interior, including (clockwise from upper left) density, y-component of mechanical polarization, von Mises stress, and pressure. 32

LIST OF TABLES

Table 1: Characteristics of FEG depoling and capacitor charging data from Bartkowski and Berning (2017) [1], corresponding to Figure 2. 12
Table 2: ALEGRA-FE input material parameters obtained from material characterization of Section 3. 25
Table 3: FE-AFE Ceramic model properties inherited from Drumm (2013) [16], unmodified by the characterization done in this work. 26
Table 4: Simulation output compared to experimental data 30

This page left blank

ACRONYMS AND DEFINITIONS

Abbreviation	Definition
AFE	Anti-ferroelectric
ALE	Arbitrary Lagrangian-Eulerian
ALEGRA	Arbitrary Lagrangian-Eulerian General Research Application
BB2017	Bartkowski and Berning (2017), reference [1]
FE	Ferroelectric
FEG	Ferroelectric generator
P-E	Polarization-electric field
PZT	Lead zirconate titanate
QSE	Quasi-static electric
QSEM	Quasi-static electromechanical

1. INTRODUCTION AND BACKGROUND

Bartkowski and Berning (2017) at the U.S. Army Research Laboratory demonstrated that an explosive charge could be used to depole a ferroelectric ceramic material and quickly transfer charge to a capacitor bank. [1] This followed decades of experimental and theoretical work that described the phenomenon of ferroelectricity, developed and characterized ferroelectric materials, and demonstrated the engineering utility of the ferroelectric generator (FEG) as a device for long-term storage and prompt, on-demand release of electrical energy. [2]-[4] Among other materials, experimental and theoretical studies over the years focused on various forms of the ferroelectric ceramic lead zirconate titanate (PZT), developed at Sandia National Laboratories, including most commonly a variety with a Zr:Ti ratio of 95:5, known as PZT 95/5. [5]-[6]

This material was the subject of extensive testing and characterization, and was the material used in the experiments of Bartkowski and Berning (2017) [1] (henceforward BB2017). A significant body of knowledge already existed on the properties and behavior of PZT 95/5 at the time of the BB2017 experiments. However, a detailed prediction of its behavior in these particular experiments could not be made at the time because (1) some material properties peculiar to the specific PZT 95/5 samples used by BB2017 were still unknown, and (2) no numerical modeling had been undertaken to evaluate PZT 95/5 properties for the unique shock loading environment of the BB2017 experiments. Therefore, a clear need existed for detailed material characterization and computational modeling.

As further motivation for materials characterization and modeling, the BB2017 experiments showed a deficit of roughly 20% in the PZT 95/5 voltage output relative to that predicted by a straightforward evaluation of the theoretical maximum. This raised questions as to the efficiency of the FEG for energy storage, and the engineering optimization of shock loading configurations.

The purpose of the study described here was (1) to measure the most important unknown properties of the PZT 95/5 material used in the BB2017 tests, including the remanent polarization, and (2) to develop a preliminary three-dimensional simulation of one of those tests, using these properties, in the ferroelectricity-enabled finite-element code ALEGRA-FE.

The remainder of this report is organized as follows. First, the BB2017 experiments are reviewed. Second, tests for experimental characterization of the PZT 95/5 material are described. Third, the ALEGRA-FE code and its capabilities are outlined, and the setup of the simulation for BB2017 tests is described. Finally, the ALEGRA-FE simulations themselves are examined, and comparisons are made to the BB2017 test results.

2. REVIEW OF PREVIOUS EXPERIMENTAL TESTS

The BB2017 experiments paired a bar-shaped FEG made of PZT 95/5 ferroelectric ceramic with a 3-inch-by-6-inch sheet of Primasheet 1000 explosive sandwiched between steel plates. Several spatial configurations of the explosive sandwich relative to the FEG bar were studied. In all cases, the shock wave from detonation of the explosive sheet provided the mechanical acceleration to depole the FEG, and charge from depolarization was collected in a circuit coupled to opposing long faces of the FEG bar via conducting electrode surfaces.

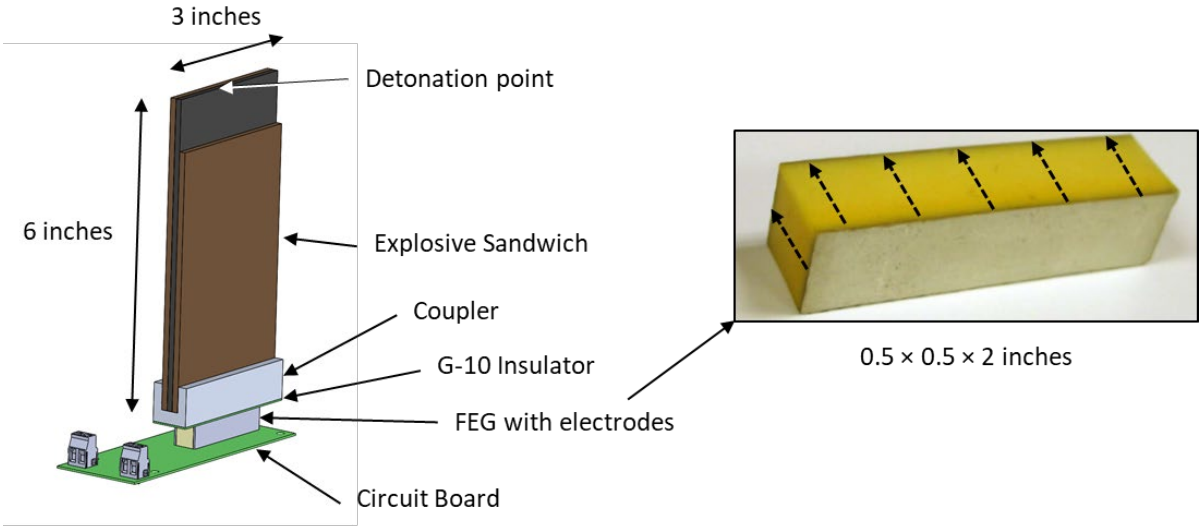

Figure 1: Reproduced from Bartkowski and Berning (2017) [1]: layout of "edge"-configuration tests (not to scale) with inset photograph of FEG bar and overlaid dashed arrows indicating the direction of the average remanent polarization direction.

In this preliminary study, we consider only the tests conducted in the "edge" configuration, shown in Figure 1. Here, the experiment starts with the initiation of an RP-80 detonator at the upper center location indicated in Figure 1. A detonation wave traverses the length of the explosive sandwich downward from the top, driving a shock wave into the coupler bracket and G-10 insulator plate at the bottom. The shock wave then interacts with the FEG, with the shock wave motion generally oriented normally to the long axis of the FEG.

The FEG itself is a bar of PZT 95/5, 12.7 mm square in cross section and 50 mm long, with superficial conducting electrodes on opposing long surfaces. The composition and thickness of these electrodes are not known, although the thickness is less than 0.1 mm. The PZT 95/5 is initially poled, on average, in the direction from one electrode to the other, as shown in Figure 1. In this configuration, the FEG is said to be "normally poled" or in "lateral orientation," in the sense that the shock wave motion is normal to the poling direction. Alternatively, or the device is called a "transverse" FEG.

An output voltage is induced in the FEG because of the ferroelectric-to-antiferroelectric (FE-AFE) phase change that occurs very quickly in the PZT 95/5 material as the shock wave of sufficient strength passes over it. The ferroelectric material an initial or "remanent" polarization P_r as ferroelectric dipoles are being poled and aligned in the electric field direction during the manufacturing process. This polarization is expressed as a scalar with units of charge per unit area normal to the polarization axis. During the shock-induced phase change, this remanent polarization is released when dipoles in the adjacent cells are coupled into a smaller volume antiferroelectric phase, and the stored charge associated with it is abruptly released and collected on adjacent electrodes feeding it into a connected circuit. The connected circuit feeds the charge to a capacitor bank which quickly becomes energized with stored charge as a result of the depoling event.

Assuming the remanent polarization is fully converted to released charge, the maximum total charge fed to the circuit can be computed from the remanent polarization simply as $Q_{max} = P_r A$, where A is the electrode surface area. BB2017 reported that the FEG manufacturer measured a remanent polarization of P_r = 33 μC/cm^2 for this material. Using the dimensions listed above, this yields a maximum theoretical charge release of Q_{max} = 209.6 μC.

Since the BB2017 experiments used a capacitor bank with total capacitance C_b = 188 nF, and the FEG itself had a capacitance of C_F = 1.25 nF, the theoretical maximum capacitor voltage resulting from the depoling event is given by

$$V_{C,max} = \frac{Q_{max}}{C_b + C_F} = \frac{P_r A}{C_b + C_F} \tag{1}$$

This yields a maximum theoretical charged capacitor voltage of $V_{C,max}$ = 1107 Volts. This expression is consistent with the final state of the capacitor predicted as an aside in Equation 36 of the theoretical analysis of Grinfeld and Grinfeld (2019). [7]

The timing of the charge collection is also of interest. For the Primasheet 1000 explosive, a nominal detonation wave speed of 7000 m/s can be assumed (from tabulated Jones-Wilkins-Lee data for EL-506CA in ALEGRA and CTH). An estimate for the onset of depoling could be obtained by neglecting wavefront curvature and computing the detonation wave traversal time for the 6-inch-long explosive sandwich. Including the 0.8-mm-thick insulator in this distance, we find a total traversal time of 21.9 μs. The RP-80 detonator used in the experiments has a function time of 2.65 μs. [8] Including this function time, we expect that shock arrival at the FEG, and initiation of capacitor charging, should occur approximately 24.5 μs after the initiation signal is sent to the detonator.

BB2017 also assumed an acoustic wave speed of 4.2 km/s in PZT 95/5. Assuming the FE-AFE phase change takes place entirely during the transit time of the shock wave across the short 12.7-mm dimension of the FEG, we can easily compute an approximate depoling voltage rise time. We find that depoling should be complete after a time interval of approximately 3 μs, or 27.6 μs after initiation of the experiment.

In the BB2017 experiments, three tests were conducted successfully in the lateral orientation: Shots 1, 3, and 5. The capacitor voltage traces from these tests are shown in Figure 2. We see that

depoling begins at approximately 25 μs as predicted, and the resulting ramp-up in capacitor voltage is linear with a slightly larger rise time of 3.3 μs. The voltage remains at a nearly steady plateau subsequently, for at least another 5 μs. This "steady-state" voltage is approximately 887 Volts. All of these characteristics extracted from the three shots are summarized below in Table 1.

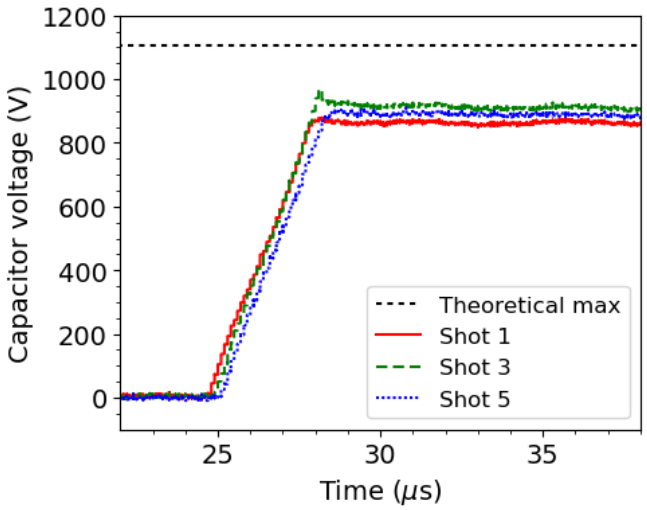

Figure 2: Reproduced from Bartkowski and Berning (2017) [1]: capacitor charging by FEG depoling, from the three successful shots in lateral orientation from the BB2017 experiments.

However, this voltage is more than 20% lower than the 1107 Volts expected based on the manufacturer's reported remanent polarization of 33 μC/cm^2. This deficit was discussed also by BB2017, noting that in none of the tests was more than 81.2% of the theoretical available charge transferred to the capacitor. By inverting Equation 1, we compute an effective charge transfer of only 26.4 μC/cm^2. BB2017 noted that loss mechanisms at play in this system are not understood, and for that reason, the present study was initiated, seeking an improved characterization of the material, and a computational model in the ALEGRA-FE code.

Table 1: Characteristics of FEG depoling and capacitor charging data from Bartkowski and Berning (2017) [1], corresponding to Figure 2.

	Shot 1	Shot 3	Shot 5	Mean	Theoretical	Difference
Shock arrival time (μs)	24.8	24.9	25.1	24.9	24.54	1.6%
Full charge time (μs)	28.05	28.15	28.50	28.23	27.56	2.4%
Rise time (μs)	3.3	3.3	3.4	3.3	3.02	9.1%
Full charge voltage (V)	862.9	911.0	887.0	887.0	1107	-19.9%
Voltage std. deviation	0.55%	0.60%	0.63%	0.59%		

3. PZT 95/5 CHARACTERIZATION TESTING

To investigate the properties of the PZT 95/5 material tested by BB2017, one representative specimen was selected out of the lot of FEG bars from which the BB2017 test samples were drawn. It was transported to Sandia National Laboratories for ferroelectric characterization. The specimen was cut into four equal pieces (cuts normal to the electrode surfaces), as shown in Figure 3. A mean density of 7744 ± 7 kg/m^3 was measured, and a mean relative permittivity of 281 ± 3, averaged over the four samples. It was also noted that after slicing, one of the four samples showed some evidence of electrocoloration [9], which could have resulted from the original poling process. All of the FEG bars in the lot were reportedly poled at least 10 years previously. [10]

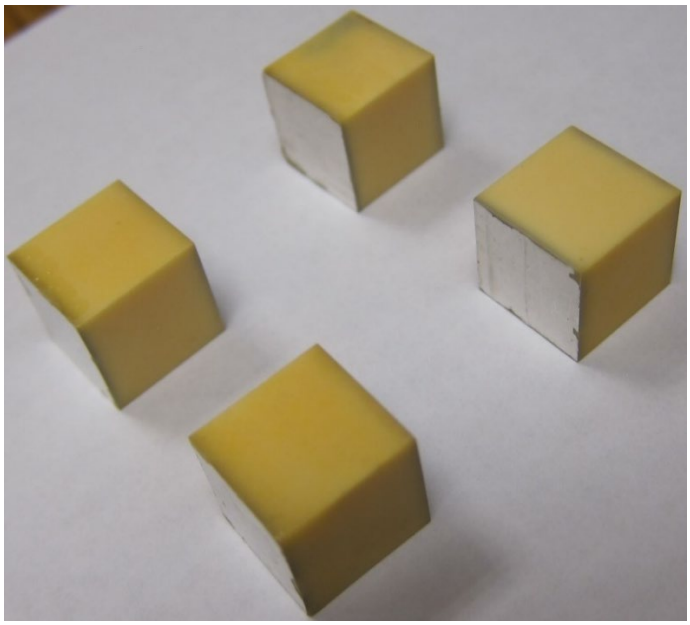

Figure 3: FEG sample after cutting into four pieces. The topmost sample shows evidence of possible electrocoloration [9].

Each of the four FEG samples was subjected to three types of tests: (1) P-E (polarization-electric field) hysteresis looping, (2) hydrostatic depoling, and (3) P-E hysteresis looping after depoling. These tests are described here, and the results of the testing, as they were used for ALEGRA-FE simulations, are summarized below in Table 2.

3.1. P-E hysteresis looping

P-E hysteresis looping refers to the measurement of the polarization in a ferroelectric material while varying an applied electric field in a cycle that captures a characteristic loop shape when plotted on axes of polarization P versus applied electric field E. An apparatus for conducting this measurement, during hydrostatic depoling if necessary, exists at Sandia National Laboratories and is

based on a modified Sawyer-Tower circuit. [11] In the Sandia apparatus, the field-induced strain is measured by a differential variable reluctance transducer (DVRT) simultaneously, as the material expands and contracts slightly during polarization reversal in the poling process.

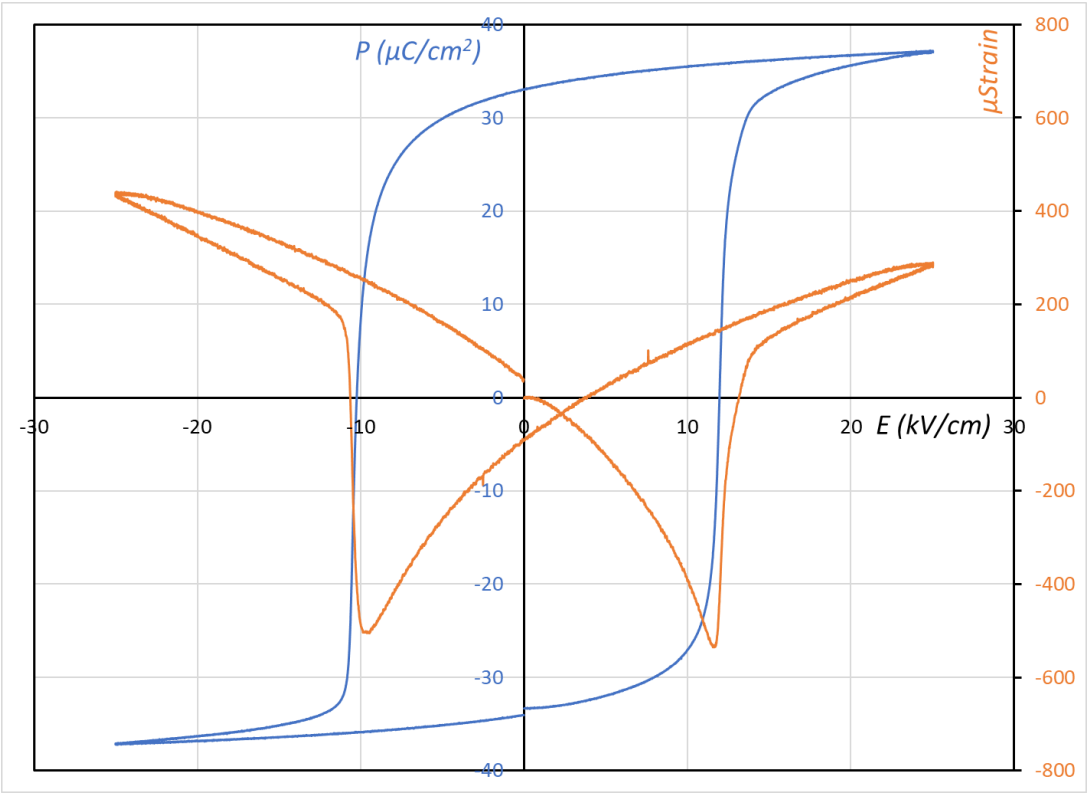

Figure 4: P-E hysteresis loop for one PZT 95/5 sample.

An example P-E hysteresis loop obtained in the second cycle of such a measurement for one of the four samples is shown in Figure 4. An initial cycle effectively repoles the sample, increasing the polarization from the as-received value P_r^0 to the repoled value P_r. In this second cycle, the blue curve traces the polarization in the counter-clockwise direction, originating from and terminating on the $E = 0$ axis at the bottom of the polarization axis (P). Similarly, the orange curve traces the strain. The remanent polarization is indicated by the point on the P axis at which the blue curve terminates. For this sample it was $P_r = 33.6$ μC/cm^2. The average value over all four samples was 33.6 ± 0.4 μC/cm^2, which is remarkably close to the manufacturer's reported remanent polarization of 33 μC/cm^2. However, the average as-received polarization over all four samples was 31.15 ± 0.24 μC/cm^2, which is lower by about 7%, indicating perhaps some aging effect. This may partially explain the deficit in transferred charge observed in the BB2017 tests.

Also indicated on the P-E looping plot is the "coercive field," which is indicated by the points for both positive and negative applied electric field at which the P-E curve crosses the $P = 0$ axis. Since these two points do not match in the plot shown in Figure 4, the data suggest that there is a built-in internal bias in the PZT samples – the entire loop is shifted slightly to the right. We speculate that this is due to charge carrier migration during the aging process. Finally, a piezoelectric

coefficient can also be obtained from the stress curve, but it is not ultimately used for the ALEGRA-FE modeling, so is not discussed here.

3.2. Hydrostatic depoling

After hysteresis looping, with the material back in the poled state, a hydrostatic depoling test was carried out. In this test, the sample is mechanically loaded within a pressure vessel, gradually increasing the load until the FE-AFE phase change happens. The rate of charge release from the FEG is measured simultaneously, and if the transition is rapid, the pressure at which the rate reaches its maximum is said to be the hydrostatic depoling pressure. A representative hydrostatic depoling curve from one of the samples is shown in Figure 5. The accumulated charge release is traced with the blue curve, and the rate of charge release on the orange curve. For this sample, the hydrostatic depoling pressure was $p_h = 57.5$ kpsi = 396 MPa, and the total charge released was $Q_h = 25.8$ μC/cm^2. The test was conducted for two of the four samples, resulting in an average depoling pressure $p_h = 393 \pm 5$ MPa, and an average charge release $Q_h = 25.8$ μC/cm^2.

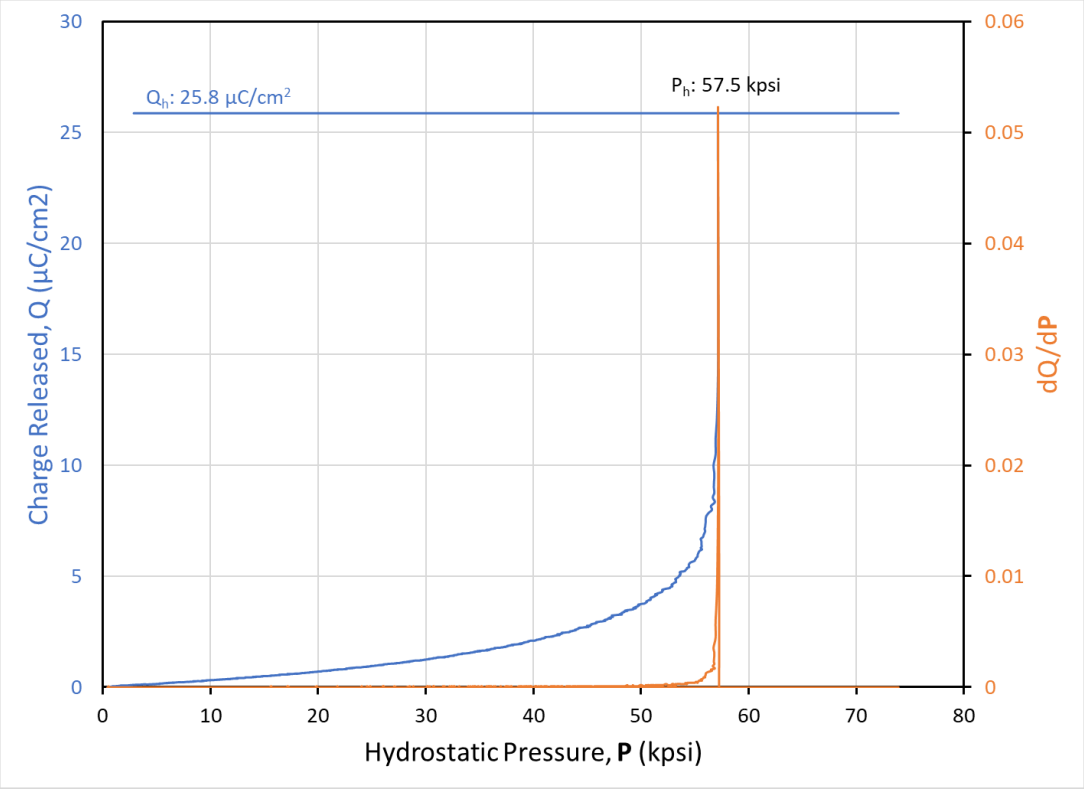

Figure 5: Hydrostatic depoling curve for one PZT 95/5 sample.

Thus, like the shock-depoling experiments of BB2017, this hydrostatic depoling test indicates a significant difference of roughly 20% between the stored charge indicated by the remanent

polarization and the charge output resulting from depoling. The charge release appears to be consistent with the output data reported in BB2017.

3.3. P-E hysteresis looping after hydrostatic depoling

To check whether there is any remaining charge that was not released in the hydrostatic depoling test, a third P-E hysteresis looping test was conducted immediately afterward for these two samples. Data from one of these tests are shown in Figure 6.

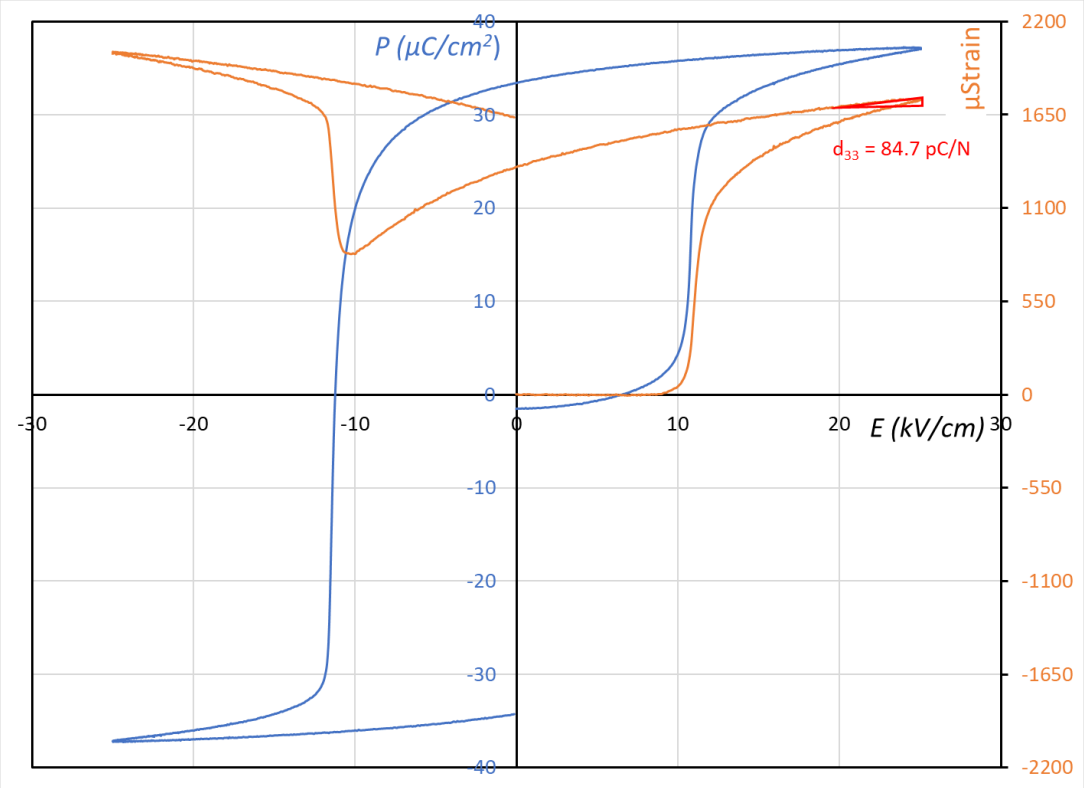

Figure 6: P-E hysteresis loop test after hydrostatic depoling.

The loop originates from a location near $P = 0$. This and the shape of the loops indicates that the material has been depoled, and all the charge stored on the PZT ceramic was almost completely released. The hysteresis looping experiment repoles the material, returning it to a polarization near the value obtained from the second loop. The hysteresis loop is now symmetrically centered about $E = 0$, confirming that there was an internal bias in the samples as received.

Further investigation into the properties of this PZT 95/5 material is needed. The loss of charge in the depoling process has not been accounted for. The loss of charge is not apparent in data presented by Alberta *et al.* (2009) [4], even though it is likely that the same material from the same manufacturer was used for those tests. The detailed composition of the material is not completely

known, and the effects of aging are also not clear. The darkening observed near the electrodes and asymmetric loop shape obtained from the second hysteresis looping test suggest that there is some trapped charge built up due to internal field during aging, which was presumably under an open circuit condition. These trapped charges with opposite charge near to the electrodes can be neutralized at depoling or shock loading condition and reduce the overall output. Further material characterization tests could yield information in these areas to assist in clarifying the questions that remain.

4. ALEGRA-FE MODELING

To shed light on the dynamic and mechanical aspects of the BB2017 tests, a computational model of the experiments was developed using the finite-element shock-multiphysics code ALEGRA. [12] The capability for modeling ferroelectricity exists within the ALEGRA-FE module (formerly known as ALEGRA-EMMA) and the software has been used to model similar systems with success. [13]-[17]

4.1. The ALEGRA-FE code

In ALEGRA-FE, the mechanical stress tensor that drives the acceleration of nodes in the finite-element mesh is dynamically coupled to the electric field via electromechanical material constitutive response models. The electric field is obtained by solving a system of equations that embody the so-called quasistatic electric field (QSE) approximation to Maxwell's laws, in the terminology of Woodson and Melcher (2009) [18]. ALEGRA-FE joins these two models in order to simulate shock- or blast-accelerated deforming materials that have electromechanical properties such as piezoelectricity or ferroelectricity. The overall solution methodology in ALEGRA-FE is an extension of a method designed originally for the SUBWAY code by Montgomery and Chavez (1986), and their report provides a good description of the methodology [19]. Details are also available in the ALEGRA-FE user manual (limited distribution) [13].

Joining a QSE solve with the solid dynamics capability in ALEGRA, the complete method is referred to as quasi-static electromechanics, or QSEM. The arbitrary Lagrangian-Eulerian methodology in ALEGRA for solid dynamics and shock hydrodynamics is discussed in detail elsewhere [12]. It updates the kinematic displacements on each timestep assuming a fixed electric field, using a constitutive model to obtain the material stress and internal forces. The QSE solve, in turn, updates the electric field on each timestep by solving for the electric potential, assuming fixed kinematic displacements, based on a constitutive model that provides the polarization, with simultaneous coupling to a circuit model and boundary conditions on the electric displacement. The influence of the mechanical evolution of the medium on the electric field and circuit behavior, and vice versa, enters through the dependence of material stress on the electric field, and the dependence of the polarization on the current stress state.

Several limitations apply to ALEGRA-FE and the QSEM methodology it uses.

- First, the QSE approximation effectively places an upper limit on the conductivity of the materials in the simulation domain. So only dielectric materials may be considered in the QSEM domain interior. Perfect conductors may be included, but only exterior to the QSEM region of the simulation, or as boundary conditions where constant electric potential is applied. A consequence of this is that although electric charge density is included, there is no concept of electric current in the model. Dielectric materials are in fact perfectly non-conducting in the model, and dielectric breakdown is not included.

- Second, the QSE approximation also effectively eliminates the magnetic field, so electromagnetism and ferromagnetic materials are not included. The electric field is curl-free and obtained from the gradient of the electric potential.

- Third, electromechanical forces are introduced only via the stress tensor obtained from constitutive models, so electrostatic forces are also not included.

- Finally, at a practical level, the QSEM capability in ALEGRA-FE is enabled only for three-dimensional (3D) geometry, and only for a contiguous Lagrangian mesh block. Remesh and remap are not supported, nor are 2D geometries. The QSEM solve can be limited to a certain block or subregion, with constant electric potential assumed elsewhere.

4.2. The FE AFE Ceramic model

To employ ALEGRA-FE effectively for modeling ferroelectric ceramics, a specialized constitutive model for the material is required. The so-called FE AFE Ceramic model in ALEGRA-FE provides the capability to model the FE-AFE phase transformation in a shock-hydrodynamics environment. This is done in such a way that the polarization fed to the QSE solve, and the stress provided to the solid dynamics integrator, realistically capture the observed behavior of ferroelectric ceramics such as PZT 95/5. The model is described in detail in unpublished notes by Brannon (2004) [20]. Core concepts embedded in the model are also discussed in References [14] and [21]. A notional overview of the model and its usage in this study follows here.

The model has three basic components: (1) mechanical response, (2) polarization/dielectric behavior, and (3) FE-AFE phase transformation. The mechanical representation allows the user to choose between porous ceramic and non-porous material, but the non-porous model (obtained by setting the input "inelasticity" parameter IELFLG = 3) is generally used for testing purposes only. Since PZT is a porous ceramic material, the porous representation is preferable. In the porous ceramic model (IELFLG = 0), an initial porosity must be specified (POROSITY), and the mechanical response is dictated using elastic bulk and shear moduli (BKMOD and SHMOD), along with a user-controllable yield surface. These properties remain unchanged between FE and AFE states. The porous representation is governed by the so-called "CKP" model [20]. In this model, the elastic moduli degrade with increasing porosity according to an inverse exponential relationship using the input parameters RGM, RKM, RGAMM, and RKAPM. Pores shrink in compression up to a pressure set using the input parameter SC, and new pores nucleate when the tensile pressure exceeds a threshold set using the input parameter ST

The yield surface incorporates a pressure-dependent strength, which is characteristic of ceramics. By default, the shape of the yield surface is assumed to be ellipsoidal in pressure-shear space. At high pressure, the yield stress approaches a user-input von Mises yield stress value (SBY), and for pressures exceeding a specified limit (PMAX), the yield stress no longer varies with pressure. An optional hardening modulus may also be specified for more realistic inelastic behavior. In tension, a fracture stress limit is applied (PCUT), beyond which the yield stress is set to zero.

The polarization properties of the material in the FE-AFE Ceramic model are the most sophisticated part of the model, and these are based on a statistical and anisotropic representation of the material's ferroelectric domains. Poled ferroelectric material has a uniform, measurable macroscopic remanent polarization vector. But within the microstructure of the material, each of the domains may have a slightly different polarization or "dipole" orientation that is deflected from this direction, as shown in Figure 7. The macroscopic remanent polarization in the poled state arises because the domains align themselves on average with the electric field used for poling the material. But they are not perfectly or uniformly aligned, and the stochastic deflections of the polarization must be taken into account in order to develop a realistic model.

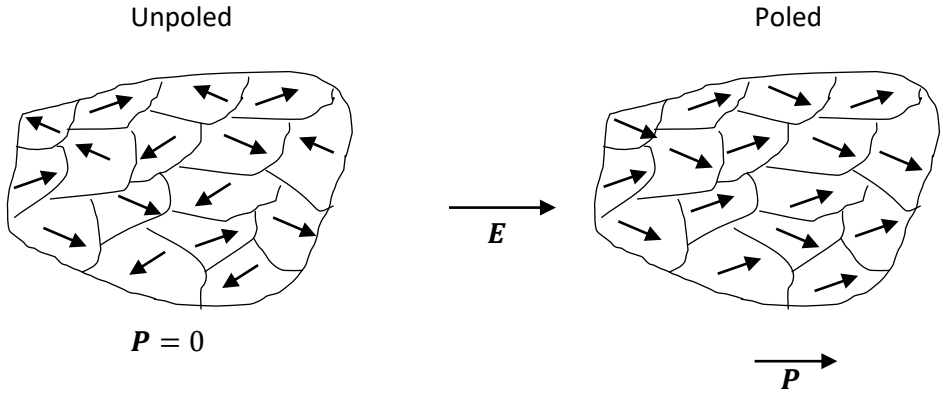

Figure 7: Notional orientation of the polarization vector in ferroelectric domains within a single grain of ferroelectric material in the unpoled (left) and poled (right) states.

In the FE-AFE Ceramic model, the deflection or "splay" of the ferroelectric domains about the input polarization vector is captured using one of two approaches which the user may select: (1) the NBINS approach, and (2) the REFINE approach. In both approaches, the solid-angle space within which domain polarization vectors may lie is discretized so that groups of polarization orientations can be tracked, without tracking each orientation individually. The two approaches are illustrated graphically in Figure 8 – taken from Reference [20].

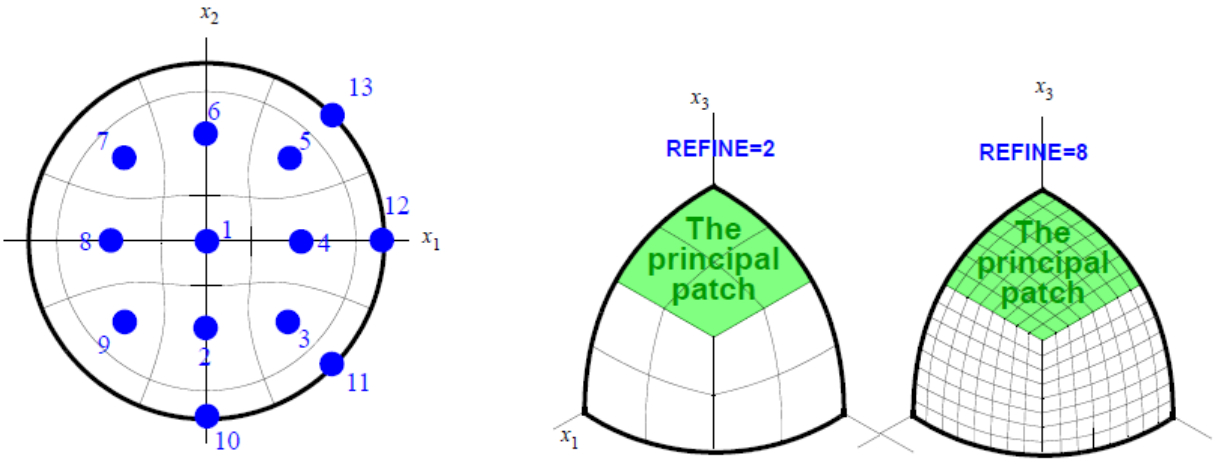

Figure 8: FE-AFE Ceramic model discretization methods for stochastic orientations of the dipoles or polarization vector: (left) NBINS approach and (right) REFINE approach. Taken from Reference [20].

In the NBINS approach, which originated with Montgomery (see Reference [14]), the unit sphere is divided into patches or "bins" of equal area. For poled material, only a 45° cone is used. The user may select the refinement of this discretization by specifying the number of bins (NBINS), which may be 1, 9 or 13. The occupancy of each bin is specified by the user with a fractional value (XN) for each of the bins; these values are also called "dipole occupancies."

In the REFINE approach, which originated with Brannon (see unpublished Reference [20]), a conical region of the unit sphere is discretized using a mesh similar to ALEGRA's "radial trisection" mesh, where a shape with radial symmetry can be constituted from topologically square patches. The user can control the level of refinement of the mesh using the REFINE keyword, but only values between 2 and 8 are allowed, and REFINE = 5 is recommended. The user also controls the angular width of the conical region using the CONANG keyword, but the recommended width is 45°.

With either approach, the average polarization is recorded in ALEGRA output field data as the element variable MECHANICAL POLARIZATION. This is actually the average over the various bins or patches, and will be uniform in space at initialization. The stochastic deflections are regarded as subgrid and are not resolved in the finite element mesh. The occupancy of the various bins in each element is only processed by the FE-AFE Ceramic material model as part of the constitutive model evaluation. Further, it is important to note that even at initialization, the MECHANICAL POLARIZATION will most likely not be colinear with the initial polarization vector specified by the user – it may point in a slightly different direction and have a slightly different magnitude, due to the nature of the solid angle discretization. Finally, it should be noted that when the inelasticity parameter is set to IELFLG = 3, in addition to omitting any porosity in the material, the model also omits all deflections in the polarization vectors.

For IELFLG ≠ 3, the stochastic deflections of the polarization affect how the ALEGRA-FE user can specify the initial polarization of the material. The macroscopic polarization differs from the polarization in individual domains by a factor that depends on the character of the splay. The FE-AFE Ceramic model requires the user to specify the single-domain polarization, P_{sd}, rather than the macroscopic remanent polarization P_r. The porosity of the material also reduces the macroscopic polarization in comparison to the single-domain polarization. To convert a measured value of P_r to a value of P_{sd} input to ALEGRA-FE, one may assume that the polarization vectors are uniformly distributed over a 45° cone. Then, for material with porosity ϕ, the single-domain polarization is

$$P_{sd} = \frac{P_r}{\xi(1-\phi)} \tag{2}$$

where the geometric factor ξ is given by

$$\xi = \frac{1}{4\left(1-\frac{1}{\sqrt{2}}\right)} = 0.853553 \tag{3}$$

To specify the initial polarization state of ferroelectric material for the FE AFE Ceramic model, a direction is specified using the [AXR, AYR, AZR] triad, and a single-domain "saturated" polarization P_{sd} is specified using the XKSAT parameter.

As for the dielectric properties of the ferroelectric material, the material does have two different values of the permittivity in the FE and AFE phases. These are regarded as fixed for each phase, and input by the user as EPSFE and EPSAF. These are absolute (not relative) permittivity values. PZT has a large relative permittivity – on the order of hundreds; porcelain, by comparison has a relative permeability of only about 6. [20] Further, since the material is anisotropic, the permittivity is a tensor. The user may specify a pair of dimensionless inputs parameters to control the anisotropy: GAM11 and GAM33. The model also includes a mechanism for breakdown. When the electric field magnitude reaches a user-specified threshold value EBRK, the permittivity is increased rapidly such that very large electric displacements quickly appear. PZT also has a very large breakdown strength, exceeding that of porcelain for example by a factor of approximately 100. [20]

The most important property of the ferroelectric material is depoling, which is the transition between the FE and the AFE phase. This transition supplies the energy to be used in the device's function as a generator. Notionally, this phase transition can be understood as the abrupt emergence, under sufficient mechanical stress, of ferroelectric domains that effectively neutralize the original polarization of their neighbors, leading to a net zero polarization in the material. This is shown schematically in Figure 9. It should be noted that although the AFE phase has a net polarization of zero, it is not equivalent to the unpoled state, in which the polarizations are oriented randomly.

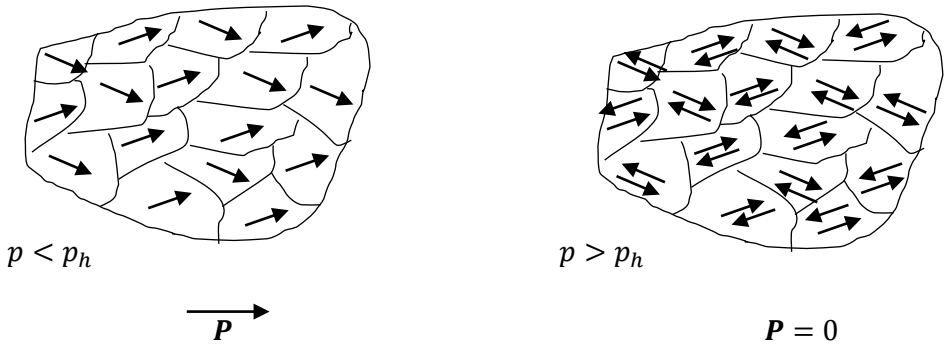

Figure 9: Notional representation of the dipoles or polarization vector in ferroelectric domains within a single grain of ferroelectric material in the FE (left) and AFE (right) states.

The FE-AFE phase change is represented in the model using a finite transition rate and a hydrostatic depoling pressure. The user input parameter ALPHA controls the transition rate, and PFE defines the pressure at which transition occurs, also called the hydrostatic depoling pressure. This pressure grows slightly with increasing temperature, with a linear coefficient defined by the input parameter SFE.

FE-AFE phase transformation introduces a disturbance in the electric displacement, which allows electric charge to accumulate on the nearest conducting boundary. This is captured naturally via the QSEM formulation in ALEGRA as a change in the electric charge on the neighboring boundary surfaces, and the electric potential on those surfaces relative to the rest of the modeled circuit network. For the conditions of this study, the transition is very fast, so that the polarization drops nearly to zero as the shock passes of over the material.

The phase transformation is also known to have mechanical effects – in particular, a volumetric strain appears at transition, which may partially attenuate the stress [14]. The magnitude of this transformation strain is specified by the user as VTRAN. Any change in elasticity of the material during transformation is not modeled and the elastic modulii are the same in the FE and AFE phases.

With all of these components together, we have the ability to model the electric output of the FEG tested by BB2017, within a larger shock-hydrodynamics simulation using ALEGRA-FE. The following section describes details of simulations where this was attempted. It should be noted that an improved model for ferroelectric materials is being developed at Sandia [22], but it is not fully available for use in ALEGRA-FE.

4.3. Simulation mesh and input parameters

The ALEGRA-FE simulations were set up on an arbitrary Lagrangian-Eulerian (ALE) mesh with about 3 million elements. The geometry and a coarsened version of the mesh is shown in Figure 10.

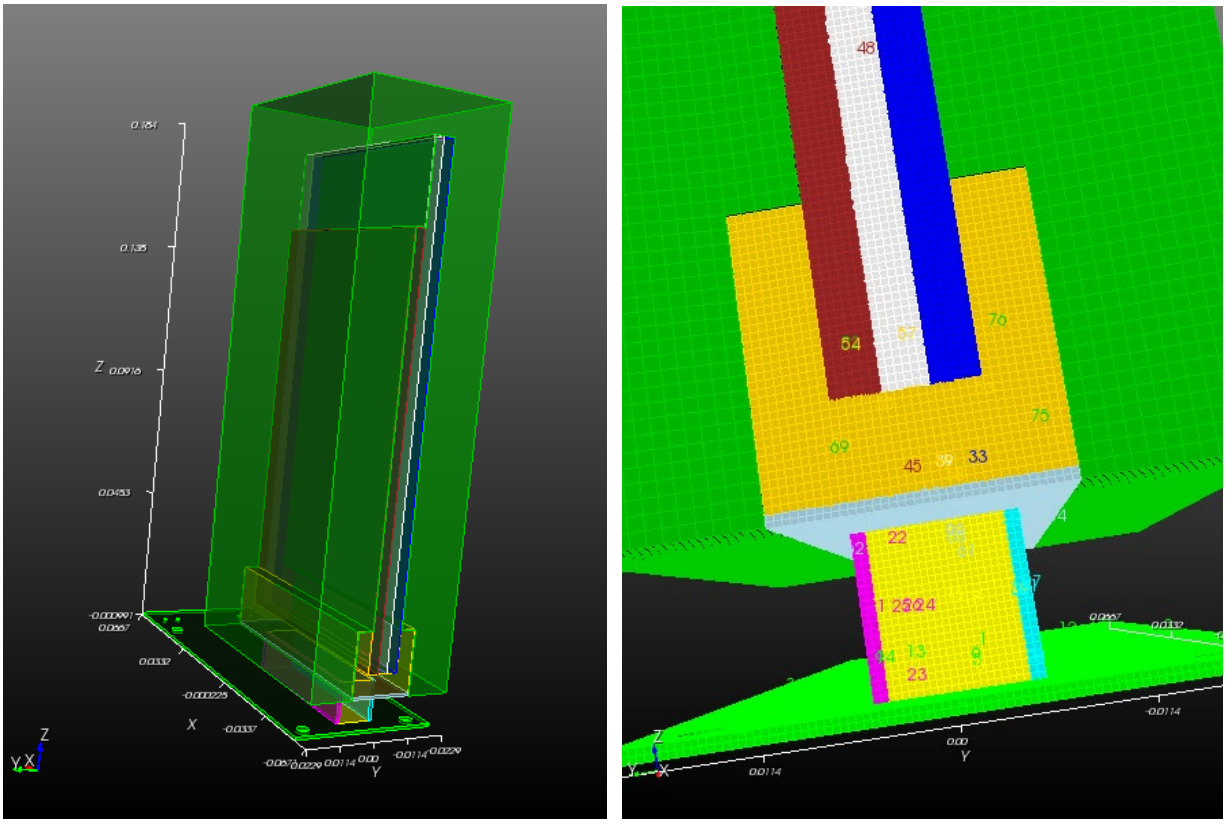

Figure 10: ALEGRA-FE simulation geometry and mesh. The mesh has been coarsened for visibility.

The simulations were configured such that ALEGRA's ALE formulation was used in the block containing the explosive, sandwich plates, and aluminum coupler bracket. This block included the

region of space where the detonation products would expand and plates would deform (shown in green in Figure 10). The remainder of the domain, including the FEG device, electrodes, G-10 insulator plate, and base plate were treated using the Lagrangian formulation. In the ALE regions, material was inserted by overlaying geometry onto the ALE mesh as volume fractions, using the Diatom algorithm of CTH and ALEGRA. In the Lagrangian regions, the mesh was body-fitted to the geometry and standard ALEGRA contact settings were used. The geometry itself was obtained from drawings made as part of the BB2017 experiments.

The dynamics of the simulation were initiated by use of a programmed burn model for the Primasheet explosive, with detonation at time zero, at a point centered at the top of the explosive sheet, opposite the FEG. The Jones-Wilkins-Lee (JWL) equation of state model was used for Primasheet, with a standard parameterization including a detonation speed of 700 m/s. For simplicity and robustness of the ALE calculation, detonation products were discarded near Eulerian domain boundaries and at very low density (volumetric expansion greater than 10,000). All explosive material was discarded 25 μs after initiation.

To pick up the electrical output of the FEG, the simulation was coupled to a lumped-element RLC circuit model. Parameters for the circuit were obtained by measurements made on the BB2017 apparatus for the present study, after the experiments were complete: $R = 44$ mΩ, $L = 849$ nH, and $C = 187$ nF, where the capacitance is associated with the capacitor bank to be charged by the FEG output. (Note that this capacitance is less by 1 nF or 0.5% than the value quoted in BB2017.) The circuit network is shown schematically in Figure 11.

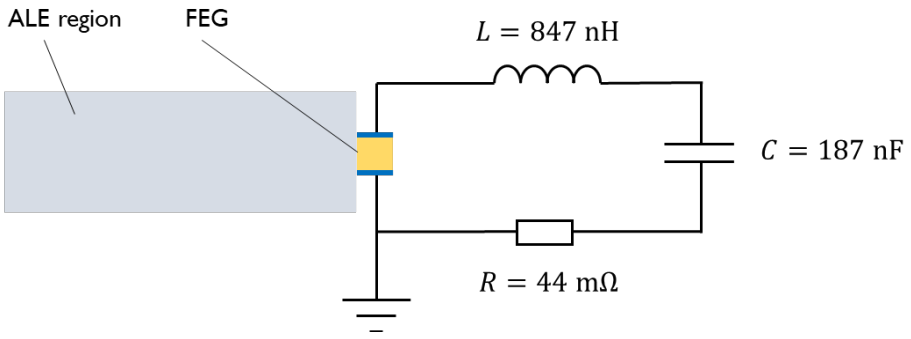

Figure 11: Circuit network used in ALEGRA-FE simulations.

4.4. Simulation material properties

The FE AFE Ceramic model was used by Drumm (2013) [16] in modeling a very similar FEG device with ALEGRA-FE. Her parameterization of PZT 95/5 was used as the starting point for the present study. Drumm's parameterization was modified based on the findings of the material characterization described in Section 3. The modified parameters are listed in Table 2.

Table 2: ALEGRA-FE input material parameters obtained from material characterization of Section 3.

Input name	Symbol	Definition	Value	Units		Value	Units
RHO INIT	ρ_0	Total (solid+void density)	7744	kg/m^3	=		
POROSITY	ϕ	Ratio of void to total volume	0.032				
-	P_r^0	As-rec'd remanent polarization	0.3115	C/m^2	=	31.15	μC/cm^2
XKSAT	P_{sd}	Single-domain sat'n polarization	0.3770	C/m^2	=	37.70	μC/cm^2
PFE	p_h	Hydrostatic depoling pressure	393	MPa	=	57.0	kpsi

For this parameterization, we note that the density of solid PZT 95/5 free of pores is assumed to be 8000 kg/m^3, and the porosity was obtained from the measured density using this value. The single-domain saturation polarization is obtained from Equations 2 and 3, based on the macroscopic remanent polarization measured on the samples as-received. The polarization direction is specified to be in the $-y$-direction, pointing from one electrode plate to the other, by setting [AXR,AYR,AZR] = [0,-1,0]. This initiates the transversely poled orientation used in the BB2017 experiments.

The measurement uncertainties in the material constants (mentioned above in Section 3) are not accounted for in the ALEGRA-FE modeling done here. These uncertainties are significant, as are uncertainties in many of the FE-AFE Ceramic inputs. ALEGRA includes the ability to propagate these uncertainties to the solution fields via ensemble studies, but this has been left for future work.

For the polarization deflection ("splay") settings in the modeling here, three configurations are used:

(1) REFINE configuration with REFINE = 8 and IELFLG = 0 (porous material)
(2) NBINS configuration with 9 bins and IELFLG = 0 (porous material)
(3) IELFLG = 3 (nonporous material, no splay)

In configuration 1, the dipole occupancies for all 9 bins (XN01 through XN09) were set equal to 0.108917. Configuration 3 was used only for testing and comparison purposes. Without porosity and polarization deflections, the algorithm does not have internal consistency and realistic results should not be expected. The porous density was still used for the material in this case.

Other FE-AFE Ceramic model parameters used for PZT 95/5 here are listed in Table 3. These were inherited from the parameterizations used by Drumm [16], and were not modified by the characterization discussed in Section 3. It should be noted that the model parameters shown here do not provide a complete set of input parameters for the FE-AFE Ceramic model – the complete list is lengthy and the rest of the parameters (in particular, the CKP porosity model parameters) are omitted here for brevity.

Table 3: FE-AFE Ceramic model properties inherited from Drumm (2013) [16], unmodified by the characterization done in this work.

Input name	Symbol	Definition	Value	Units
--[Mechanical]--				
BKMOD	K	Bulk modulus	189e9	Pa
SHMOD	G	Shear modulus	98.8e9	Pa
PCUT	-	Fracture stress limit	0.15e9	Pa
PMAX	-	Pressure-dependent yield stress limit	0.80e9	Pa
SBY	Y	von Mises yield stress at high pressure	1e12	Pa
TEMP		Room temperature	23	°C
--[Electrical]--				
EPSFE	ε_{FE}	Permittivity in FE phase	3.1e-9	F/m
EPSAF	ε_{AFE}	Permittivity in AFE phase	2.79e-9	F/m
GAM11	-	Scaling parameter for axial permittivity	0.34	-
GAM33	-	Scaling parameter for axial permittivity	-0.12	-
EBRK	-	Breakdown electric field magnitude	6e+8	V/m
--[Phase transition]--				
VTRAN	-	Transition strain	0.0035	-
SFE	-	Thermal enhancement rate of PFE	8.4e-7	Pa/K

Aside from PZT 95/5 and explosive, the simulations also include steel plates, aluminum coupler bracket, aluminum electrode plates, G-10 fiberglass insulator plate, and circuit board plate. Steel is modeled using the Mie-Grüneisen EOS and the Steinberg-Guinan-Lund yield model. Aluminum is modeled using the Mie-Grüneisen EOS for aluminum 6061 and the Johnson-Cook yield model. The insulator and circuit board plates are modeled crudely as polymethylmethacrylate (PMMA), with the Mie-Grüneisen equation of state (EOS), an elastic-perfectly-plastic model, a yield stress of 1 GPa, and a Poisson's ratio of 0.38.

4.5. Caveats related to the simulations

Two important caveats about the simulation setup became important. First, the thickness of the electrode plates at the ±y-surfaces of the PZT material was assumed to be 1 mm, which is quite large. Later measurements indicated that the electrodes were in fact merely superficial coatings, less than 0.1 mm in thickness. Since the outer dimension of FEG was preserved in the simulation, about 1.8 mm of PZT material was absent in the poling direction. This does not affect the cross sectional area for electric displacement. Second, the G-10 insulator plate was misplaced in the mesh by a downward z-displacement equal to its thickness. This allowed it to slip past the FEG after the shock arrival, without triggering contact forces. Hence, the mechanical effect of the insulator plate was lost in these simulations.

5. SIMULATION RESULTS

ALEGRA-FE simulations using the setup described above with configuration 1 (REFINE) and 2 (NBINS) were run to a simulation time of 40 μs on 256 processors for the "edge shock" setup of BB2017. An overview of the dynamics of the NBINS simulation is shown in Figure 12. As described in Section 2, in the "edge" configuration of BB2017, the shock wave requires more than 20 μs to reach the FEG after initiation at the top center. This delay is visible in these images, showing that no motion of the coupler or FEG is visible until after t = 20 μs. Depoling takes place in the following 15 μs, and at t = 35 μs, the coupler (purple) has been substantially deformed, and the FEG (pink) has also moved. Explosive material and detonation products are no longer visible in the last frame because they are discarded at t = 25 μs.

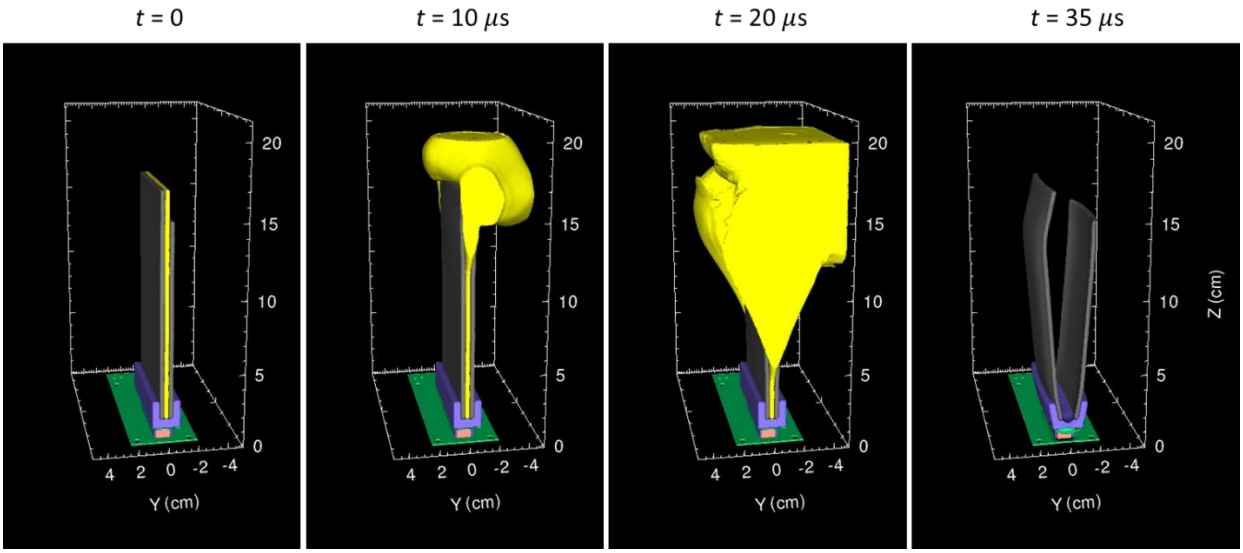

Figure 12: Material motion in ALEGRA-FE simulations using configuration 1. Yellow: explosive (discarded at t = 25 μs). Green: fiberglass modeled as PMMA. Gray: steel. Purple: aluminum. Pink: PZT.

The traversal of the shock wave over the FEG bar from this simulation is shown in Figure 13. The graphs show the y-component of the average polarization vector (MECHANICAL POLARIZATION) on a slice through the domain at the midplane of the explosive assembly. Prior to shock arrival, the y-polarization appearing in the plots is -0.30 C/m^2. (See also Figure 16 below.) We note that this is smaller in magnitude than both the single-domain value (P_{sd} = 0.3770 C/m^2) imposed in the input file, and the associated as-received remanent polarization value (P_r^0 = 0.3115 C/m^2) obtained from our material characterization. The value is slightly smaller because of the polarization splay, which deflects some portion of the polarization into the x- and z- directions, based on the deflection bin occupancy values specified in the simulation input.

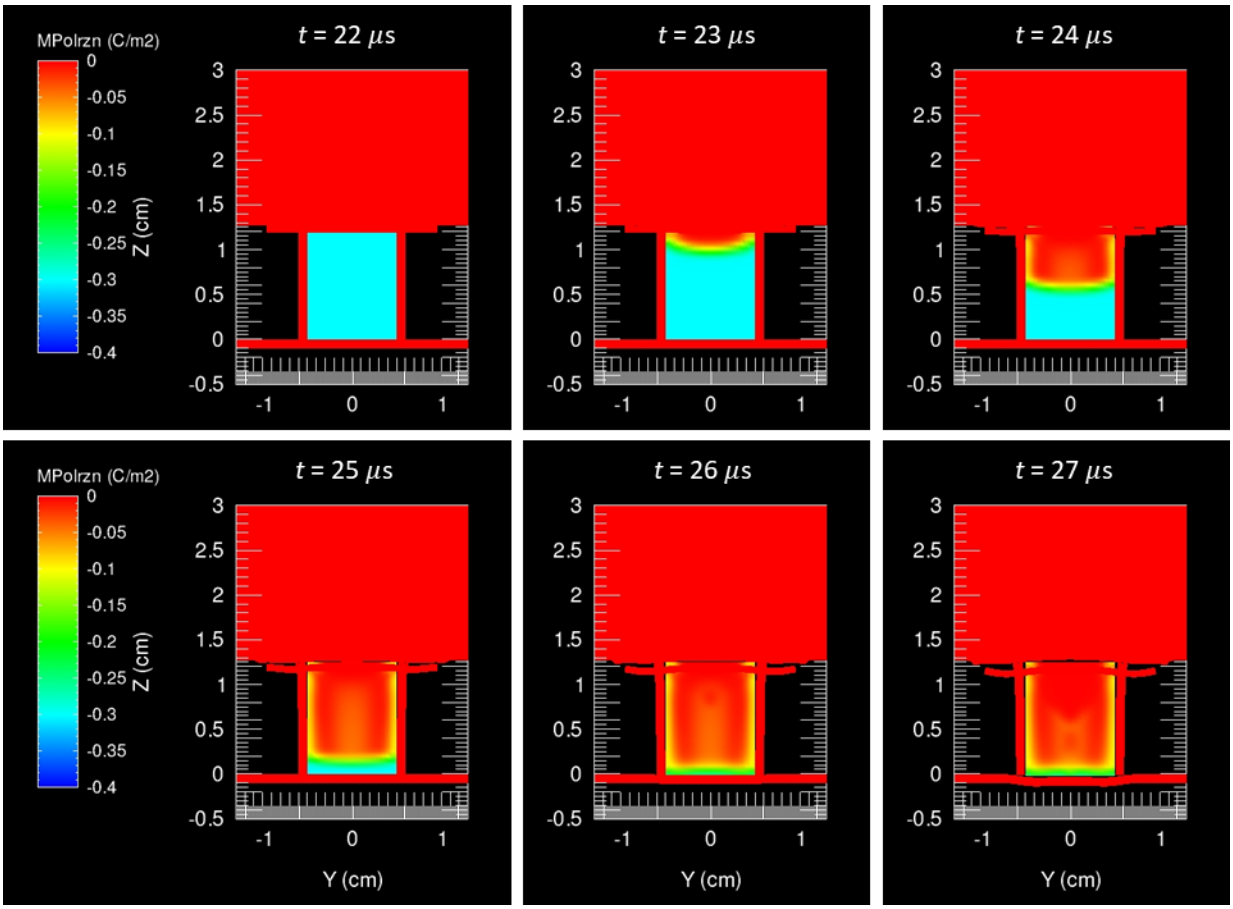

Figure 13: Mechanical polarization *y*-component evolution during shock traversal over the FEG.

The shock wave arrives at the upper surface of the FEG at approximately $t = 22.5\ \mu s$. After correction for the RP-80 detonator function time, this corresponds to an arrival time of 25.2 μs in the timeframe of the experimental measurements. This differs from the experimental and theoretical values listed in Table 1 by approximately +1%. The shock traverses the FEG in approximately 5 μs, and over that time the polarization quickly drops to values near zero, in the interior of the FEG. On the FEG surfaces that are not bounded by void, a thin sheath of weak nonzero polarization lingers after shock traversal, but for practical purposes, the FEG is effectively depoled. The resulting disruption of the electric displacement field causes charge accumulation on the electrode plates. The circuit model responds by passing this charge to the plates of the capacitor shown in the circuit network in Figure 11. The voltage across the capacitor rises abruptly as depoling progresses and charge accumulates, reaching a sustained plateau near 1 kV.

Time histories of output voltage and capacitor voltage in the ALEGRA-FE circuit model during depoling are shown in Figure 14 for three different configurations of the FE-AFE Ceramic model. The three experimental shots from BB2017 in "edge" configuration, and the maximum theoretical output from Equation 1, are also shown for reference. In each configuration, the stochastic deflections or "splay" of the polarization is handled differently, and described in Sections 4.2 and 4.4:

- "Fine splay": REFINE approach with 8 levels of refinement.
- "Splayed": NBINS approach with 9 occupancy bins.
- "No splay": IELFLG = 3.

The output voltage is the electric potential on the circuit terminal connecting the FEG electrode to the circuit model. The capacitor voltage is the voltage drop across the capacitor. There is a slight difference between them because of the resistance and inductance between the FEG and the capacitor (see Figure 11). The resistance and inductance in the circuit smooth out some of the oscillations seen in the FEG output voltage.

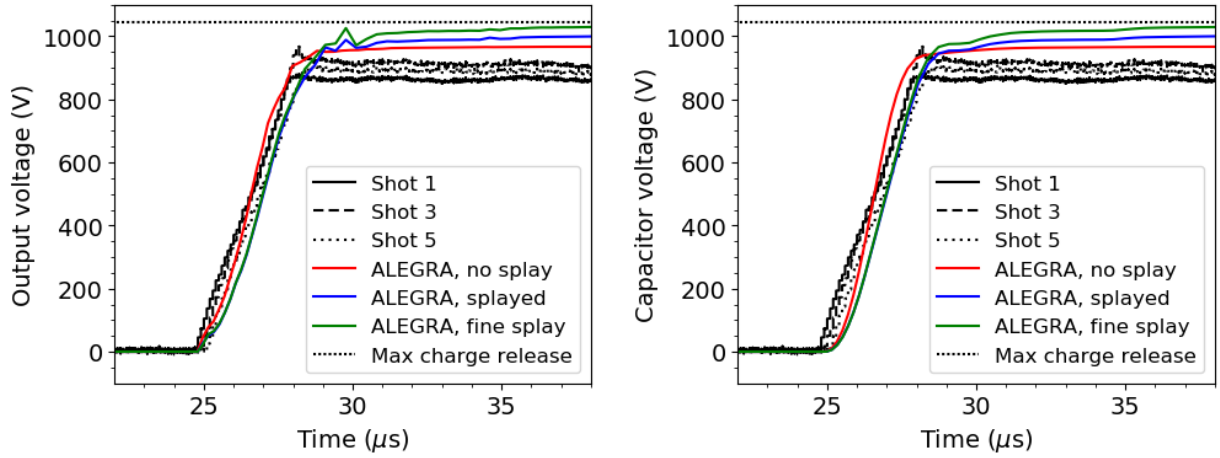

Figure 14: Measured and simulated capacitor voltage history during FEG depoling, with simulated voltages measured (left) on the FEG output terminal and (right) across the capacitor. Measured data are from the three "edge" shots from BB2017 [1].

In these plots, the simulation data have been shifted later in time by 2.65 μs (the RP-80 detonator function time). We see that in all three configurations, ALEGRA-FE, with this parameterization of the FE-AFE Ceramic model, captures the rapid charging of the capacitor bank by FEG depoling, though details of the charging history are not all resolved. Even in the relatively unrealistic configuration with no deflections of the polarization vector, the basic behavior is captured.

We also note that in all three configurations, ALEGRA predicts a final capacitor voltage that exceeds the experimental data, but remains smaller than the maximum charge release voltage of 1107 Volts predicted by Equation 1. Thus, even in the ALEGRA-FE model, not all of the stored charge is released – but more of it is released than was found by BB2017.

In Table 4, the final capacitor voltages from ALEGRA-FE are compared with those from the experimental measurements of BB2017. Shock arrival times are also measured, as the time when the FEG output electrode voltage first exceeds 10 Volts. The "final" capacitor voltage is measured as the average over the last 2 μs of the time history ($33 \leq t \leq 35$ μs). The rise time is measured as the time required after shock arrival for the capacitor voltage to reach 90% of the final value. The simulation results match the experimental and theoretical results nicely in terms of the shock arrival time, and time required to charge the capacitor. The final capacitor voltages obtained in ALEGRA-

FE simulations exceed the experimental result (mean of shots 1-3) by 9% to 16%. But they also fail to reach the theoretical maximum, like the BB2017 experiments. This suggests that the visible fringe of polarization left on the margins of the FEG after depoling in Figure 13 may contain dipoles whose charge remains bound within the material, and perhaps this effect is at play in the experiments as well.

Table 4: Simulation output compared to experimental data.

		ALEGRA			Exp'ts
	Theoretical	Fine splay (REFINE)	Splayed (NBINS)	No splay (IELFLG=3)	Shot 1-3 Mean
Shock arrival time (μs)	24.5	25.0	25.0	25.0	24.9
90% charge time (μs)	27.6	28.4	28.4	28.0	28.2
Rise time (μs)	3.0	3.4	3.4	3.0	3.3
Rise time % difference from experiments	-10%	+1%	+1%	-10%	-
Full-charge voltage (V)	1107	1028	998	966	887
Full-charge voltage % difference from exp'ts	+25%	+16%	+13%	+9%	-

It is interesting that the case of IELFLG = 3 implies no splay and no porosity, yet it has the best fidelity to the experimental results. This is most likely coincidental. Several explanations were hypothesized as to the 13% to 16% excess voltage predicted by ALEGRA-FE in the porous, splayed cases. But they are all inconclusive:

(1) Potentially insufficient mesh resolution. To test this, a subsequent calculation was done in the NBINS configuration with the mesh interval halved in each direction, resulting in 25 million elements in the mesh. This resulted in a slightly smaller rise time, but no difference in the final capacitor voltage.

(2) Incorrect electrode thickness and misplaced insulator plate. As mentioned above in Section 4.5, there were minor errors in the geometry, related to the electrode thickness and insulator plate position. In subsequent NBINS calculations, the electrode material was removed completely, and the insulator plate was repositioned. The mesh and contact settings were also adjusted accordingly. But in those cases, the rise time was nearly 5 times longer, and exhibited a stepped structure. This was apparently due to pressure reverberations associated with motion of the insulator plate, and the absence of the electrode plate inertia.

(3) Anomalously low polarization in tested FEG's. To test this, three additional calculations were done in the NBINS configuration, with the input value of XKSAT (P_{sd} = initial FEG polarization) reduced to 95%, 90%, and 80% of the value resulting from the characterization. The results shown in Figure 16 show that at 90%, ALEGRA-FE does match the experimental capacitor voltage. However, there is no apparent justification for such an *ad hoc* adjustment of the remanent polarization.

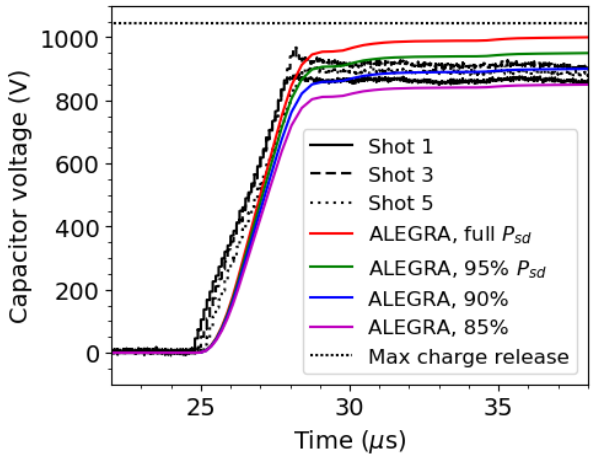

Figure 15: Capacitor voltage from simulations with reduced values of remanent polarization.

Another explanation may be hypothesized as to the excess voltage: trapped charge present in the BB2017 FEG bars prior to testing. As mentioned in Section 3.3, there were observations of discoloration in the FEG samples, and symmetry/asymmetry of hysteresis loops measured before and after hydrostatic depoling, which suggested the presence of trapped charge in the FEG bars. The presence of these charges, and their neutralization upon depoling is not captured in the ALEGRA-FE model. Whether this may account for any portion of the disparity in the results could be a topic of future research.

Additional details of the original three ALEGRA-FE simulations are shown below in Figure 16, where time-history data are plotted from a diagnostic tracer point located in the interior of the PZT material, near its geometric centroid. From these data we make the following observations:

- In the splayed, porous configurations (NBINS and REFINE), the material volumetrically contracts by approximately 1% during the shock and depoling phase, as seen in the density history. In the nonporous simulation without splay, the material contracts initially, then expands later in time.

- The mechanical polarization changes very abruptly in all three cases, but in the porous, splayed configurations, the transition includes some stepped structure. These steps correspond to times when the x- and z-components of the polarization abruptly jump, indicating additional polarization is being deflected transiently into directions oriented away from the electrodes. This effect is present in both splayed cases, but it is more prominent in the NBINS case than in the REFINE case.

- In both the pressure and von Mises stress histories, we observe that with the porous, splayed configuration, shock reverberations are quite pronounced, and the material even goes into tension in some of these reverberations. The reverberations are much less pronounced in the nonporous case.

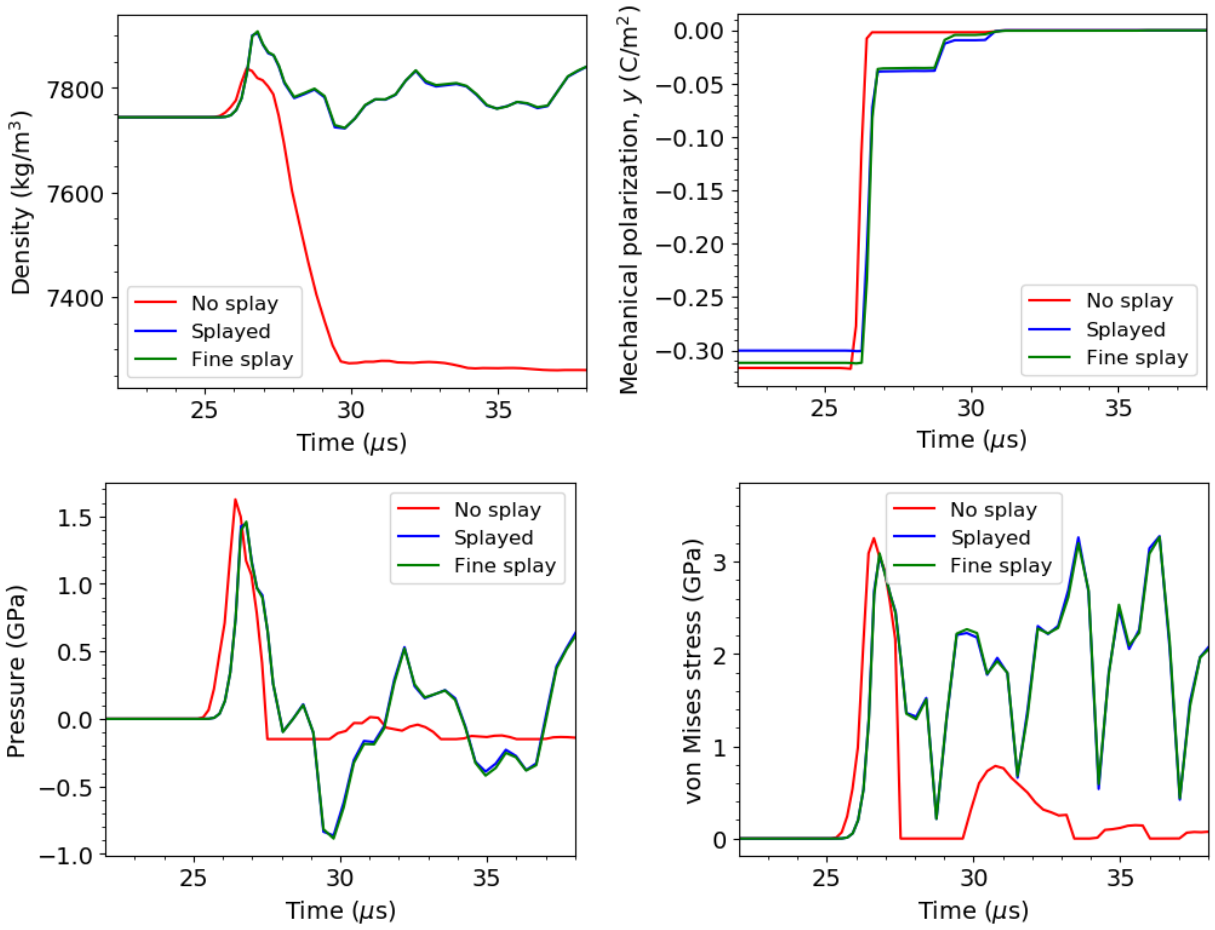

Figure 16: Time history data from a diagnostic tracer point in the FEG interior, including (clockwise from upper left) density, *y*-component of mechanical polarization, von Mises stress, and pressure.

6. CONCLUSIONS

A complete numerical model for the ferroelectric-generator experiments of Barkowski and Berning (2017) [1] was constructed in this work, including material characterization, material model parameterization, meshing, and simulation. The results demonstrate that ALEGRA-FE provides a reasonable approximation to the important mechanisms at play, including fully coupled shock hydrodynamics and ferroelectricity. The simulations capture the charging of a capacitor bank by depoling a FEG, with rise time captured to within 10% and final voltage captured to within about 15%.

The results do not provide a conclusive explanation for the deficit in FEG output voltage observed in the 2017 experiments. But they do show that the theoretical maximum output is also not achieved for the simulated material. The materials characterization conducted suggests that other effects may be at play including trapped charge in the FEG material.

Some improvements upon this work are suggested. In particular, corrections to the placement of the insulator plate and the electrode thickness should be incorporated into the model, and a more comprehensive set of simulations on a finer mesh should be completed.

The simulations and related analysis pave the way for further work in this area. ALEGRA-FE simulations should be conducted for the "side" geometry of the BB2017 work. New material characterizations and simulations could also prove helpful as new FEG designs are manufactured and tested. Finally, we anticipate continued constructive feedback to the development of the ALEGRA-FE code and its material models from validation studies such as this.

REFERENCES

[1] P. Bartkowski and P. Berning, "The Use of Ferroelectric Ceramics to Charge Small Capacitor Banks," US Army Research Laboratory technical report ARL-TR-8140, September 2017.

[2] J. R. Asay, L. C. Chhabildas, R. J. Lawrence, and M. A. Sweeney, *Impactful Times: Memories of 60 Years of Shock Wave Research at Sandia National Laboratories*, Springer, 2017.

[3] L. L. Altgilbers, "Explosive pulsed power: an enabling technology," In Proc. 26th Army Science Conference, 2008.

[4] E. F. Alberta, B. Michaud, W. S. Hackenberger, B. Freeman, D. J. Hemmert, A. H. Stults, and L. L. Altgilbers, "Development of ferroelectric materials for explosively driven pulsed-power systems," In Proc. 17th IEEE International Pulsed Power Conference, 2009, pp. 161-166. https://doi.org/10.1109/PPC.2009.5386193

[5] R. E. Setchell, "Shock wave compression of the ferroelectric ceramic $Pb_{0.99}(Zr_{0.95}Ti_{0.05})_{0.98}Nb_{0.02}O_3$: Hugoniot states and constitutive mechanical properties," Journal of Applied Physics **94**, 573 (2003).

[6] R. E. Setchell, "Shock wave compression of the ferroelectric ceramic $Pb_{0.99}(Zr_{0.95}Ti_{0.05})_{0.98}Nb_{0.02}O_3$: Depoling currents," Journal of Applied Physics **97**, 013507 (2005).

[7] M. Grinfeld and P. Grinfeld, "Circuit models of pyroelectric charger," US Army Research Laboratory technical report ARL-TR-8669, March 2019.

[8] RP-80 EBW detonator documentation, Teledyne RISI, http://www.teledynerisi.com/products-services/ebw-detonators/rp-80-ebw-detonator

[9] H. Ossmer, C. Slouka, L. Andrejs, P. Blaha, G. Friedbacher, and J. Fleig, "Electrocoloration of donor-doped lead zirconate titanate under DC field Stress," Solid State Ionics **281** 49-59 (2015). https://doi.org/10.1016/j.ssi.2015.08.021

[10] P. Bartkowski and P. Berning, private communication, April 5, 2018.

[11] C. DiAntonio, W. Dong, T. Hughes, T. Chavez, L. Haden, P. Yang, and K. Meyer, "Exploring the evolution of the polarization behavior for Nb-PZT based on the electric field-pressure conditions," 18th US-Japan Seminar on Dielectric & Piezoelectric Materials, November, 2017 (SAND2018-0956C).

[12] A.C. Robinson, T. A. Brunner, S. Carroll, and coauthors, "ALEGRA: An arbitrary Lagrangian-Eulerian multimaterial, multi-physics code." In: Proc. 46th AIAA Aerospace Sciences Meeting: AIAA-2008-1235, 2008.

[13] S. W. Bova, J, B. Carleton, J. H. J. Niederhaus, A. C. Robinson, M. K. Wong, and W. D. Dong, "User manual for ferroelectric (FE) modeling in ALEGRA," Sandia National Laboratories technical report SAND2019-0785, 2019. (Limited distribution.)

[14] R. M. Brannon, S. T. Montgomery, J. B. Aidun, A. C. Robinson, "Macro- and meso-scale modeling of PZT ferroelectric ceramics," AIP Conference Proceedings **620**, 197, 2002. https://doi.org/10.1063/1.1483514

[15] M. D. Furnish, J. Robbins, W. M. Trott, L. C. Chhabildas, R. J. Lawrence, and S. T. Montgomery, "Multi-dimensional validation impact tests on PZT 95/5 and ALOX," AIP Conference Proceedings **620**, 205, 2002. https://doi.org/10.1063/1.1483516

[16] M. C. Drumm, "Computational simulation of explosively generated pulsed power devices," M.S. thesis, U.S. Air Force Institute of Technology, 2013.

[17] S. Kaplan, "Piezoelectric response of ferroelectric ceramics under mechanical stress," M.S. thesis, U.S. Air Force Institute of Technology, 2015.

[18] H. H. Woodson and J. R. Melcher, *Electromechanical Dynamics*, Massachusetts Institute of Technology: MIT OpenCourseWare, 2009. http://ocw.mit.edu

[19] S. T. Montgomery and P. F. Chavez, Basic equations and solution method for the calculation of the transient electromechanical response of dielectric devices," Sandia National Laboratories technical report SAND86-0755, 1986.

[20] R. M. Brannon, "FE/AFE analysis at Sandia National Laboratories: a summary of equations governing the thermal, electrical, and mechanical behavior of dielectrics with emphasis on PZT," unpublished draft Sandia technical report (limited distribution), 2004.

[21] S. T. Montgomery, R. M. Brannon, J. Robbins, R. E. Setchell, and D. H. Zeuch, "Simulation of the effects of shock stress and electric field strength on shock-induced depoling of normally poled PZT 95/5," AIP Conference Proceedings **620**, 201, 2002. https://doi.org/10.1063/1.1483515

[22] W. Dong, J. Robbins, and C. DiAntonio, "General phenomenological micromechanical constitutive model for ferroelectric materials," ASME 2017 Conference on Smart Materials, Adaptive Structures and Intelligent Systems, 2017 (SAND2017-3480 A).

DISTRIBUTION

Email—Internal

Name	Org.	Sandia Email Address
Technical Library	01177	libref@sandia.gov

This page left blank.

Sandia National Laboratories

Sandia National Laboratories is a multimission laboratory managed and operated by National Technology & Engineering Solutions of Sandia LLC, a wholly owned subsidiary of Honeywell International Inc. for the U.S. Department of Energy's National Nuclear Security Administration under contract DE-NA0003525.